7-2012

Inverse Modeling to Simulate Fault Impacts for Vapor Compression Equipment Part 2: System Modeling and Validation

Howard Cheung
Ray W. Herrick Laboratories, Purdue University, howard.at@gmail.com

James E. Braun
Ray W. Herrick Laboratories, Purdue University

Inverse Modeling to Simulate Fault Impacts for Vapor Compression Equipment Part 2: System Modeling and Validation

Howard CHEUNG*, James E. BRAUN

Ray W. Herrick Laboratories, School of Mechanical Engineering, Purdue University
West Lafayette, Indiana, U.S.A
E-mail: cheung@purdue.edu

* Corresponding Author

ABSTRACT

This paper utilizes the component models described in a companion paper to develop a full system inverse model for normal and faulty performance of vapor compression cooling and heating equipment. Algorithms to simulate different faults, such as loss of refrigerant charge, compressor valve leakage, liquid line restriction, etc. are presented. Component model parameters were estimated from laboratory experimental data without complete knowledge about the component characteristics. The system model was tuned to offset the bias that resulted from model simplifications. The method was carried out with data from a 3-ton R410a packaged unit with fixed orifice expansion, operating with faults such as incorrect refrigerant charge and heat exchanger fouling. The system model outputs had good agreement with the experimental data. The impacts of faults on performance determined through simulation are also presented.

1. INTRODUCTION

Faulted conditions, such as incorrect refrigerant charge and heat exchanger fouling, have been shown experimentally (Breuker, 1997; Shen, 2006; Kim *et al*,. 2009) and by simulations (LeRoy, 1997; Shen, 2006) to deteriorate the performance of vapor compression equipment. Several fault detection and diagnostics (FDD) tools are available in the market to alert equipment operators to the presence of these faults. A current effort to develop evaluation methods for such FDD tools (Yuill and Braun, 2012) has found that reliable simulation data are needed. However, existing simulation tools for faulted conditions are too slow and labor intensive to fulfill the needs. In this paper, a component-based model is developed, which is able to estimate the operating characteristics required by FDD tools quickly and accurately to meet the needs of FDD evaluation methods.

There are a variety of faults that reduce performance in air-cooled vapor compression cycles. For example, systems under-perform if they do not have the optimal refrigerant charge level, and can damage the compressor if sufficiently overcharged (Shen, 2006). Air-side heat exchanger fouling impairs heat transfer and can decrease airflow rates across the heat exchangers, decreasing performance. Compressor valve leakage (in which the valves of the compressor wear and refrigerant cannot be discharged to the cycle completely after compression) and liquid line restrictions (which induce an unintended pressure drop between the expansion valve and condenser) also degrade system performance (Kim *et al.*, 2009).

To simulate faulted conditions, the solver needs to be able to accept the following as inputs: the amount of charge in the system, evaporator and condenser airflow, compressor valve leakage level and liquid line restriction level. Charge tuning methods to offset the aforementioned bias from existing void fraction models and inaccurate internal volumes were developed by Rossi (1995), Harms (2002) and Shen (2006). These were used with a finite-volume approach to simulate the system performance. Compressor valve leakage and liquid line restriction models were also described in Breuker (1997).

In the current paper, component models from Cheung and Braun (2012) are utilized to estimate the performance of a 3-ton R410A packaged unit with a fixed orifice, which was tested by Shen (2006). The estimation is compared with the experimental data for non-standard charging and heat exchanger fouling scenarios. Additional fault conditions such as compressor valve leakage and liquid line restriction are also simulated.

2. CYCLE SOLVERS

Since there is usually a bias between the real charge level and estimates based on void fraction models, it is necessary to conduct charge tuning on the cycle model with experimental data before the model can estimate charge accurately (Harms, 2002; Shen, 2006). Two cycle solvers are needed; one accepts superheat at the compressor outlet as an input for charge tuning with systems having an FEO, and the other receives charge as an input to simulate the cycle performance. The other inputs are the return air conditions and airflows to each heat exchanger. The arrangement of the component models in the solution process is shown in the appendix in Figure A.1.

The independent variables and imposed constraints of the solvers are listed in Table 1. The residuals, also listed in the table, are minimized by the sum-of-least-squares method to obtain a solution. The coefficients in the constraints are chosen arbitrarily, and only come into effect when an error is encountered during an unconstrained optimization process. This arrangement helps to enhance calculation speed in ordinary cases and to avoid divergence in extreme scenarios.

Table 1: Independent variables and constraints of solvers.

Inputs	Independent variables	Constraints on independent variables	Residuals
Compressor discharge superheat/ Amount of charge	$P_{r,sat,comp,out}$	Refrigerant critical pressure and saturation pressure at $T_{a,cond,in}$	$\dot{m}_{r,comp}$ - $\dot{m}_{r,FEO}$
Airflow across evaporator	$P_{r,sat,comp,in}$	Saturation pressures at $T_{a,evap,in}$ and 250 [K]	$h_{r,FEO,in}$ - $h_{r,liquidline,out}$
Airflow across condenser	$SH_{evap,out}$	None	$h_{r,evap,out}$ - $h_{r,suctionline,out}$
Return air dry-bulb temperature	$P_{r,comp,out}$ - $P_{r,FEO,in}$	5 x Maximum $P_{r,comp,out}$ - $P_{r,FEO,in}$ from experimental data and 0	$P_{r,FEO,in}$ - $P_{r,liquidline,out}$
Return air dewpoint	$P_{r,FEO,out}$ - $P_{r,suctionline,out}$	3 x Maximum $P_{r,FEO,out}$ - $P_{r,suctionline,out}$ from experimental data and 0	$P_{r,suctionline,out}$ - $P_{r,evap,out}$
Ambient dry-bulb air temperature	$SC_{FEO,in}$	None	$SH_{comp,out} - SH_{comp,out,mea}$ (for discharge superheat as an input) or M_{mea} - $M_{sim,fina}$ (for charge as an input)

The partial derivative of refrigerant mass flow rate with respect to the fixed orifice inlet enthalpy is discontinuous at zero subcooling (Payne and O'Neal, 1999) leading to potential numerical problems in the solver. Since the inverse model of the fixed orifice is generated with data for which subcooling is greater than 3K, linear interpolation is conducted to calculate refrigerant mass flow rate whenever inlet subcooling is less than 3K and inlet thermodynamic quality is less than 0.05. This smooths the iteration surface and speeds up the calculation.

3. CHARGE TUNING

A charge tuning equation was developed from Shen (2006) to account for the underestimation of charge caused by the inaccuracy in the volume and void fraction model in the simulation. Shen (2006) assumes a constant heat transfer coefficient in the charge tuning equation and the assumption is relaxed from Eq. (1), resulting in a new charge tuning equation, shown in Eq. (2).

$$M_{mea} - M_{sim,initial} = C_{0,old} + C_{1,old} w_{cond,sc} + C_{2,old} w_{cond,sh} + C_{3,old} w_{evap,sh} \quad (1)$$

$$M_{mea} - M_{sim,initial} = C_0 + (C_1 UA_{overall,cond,sc} + C_2) w_{cond,sc} + (C_3 UA_{overall,cond,sh} + C_4) w_{cond,sh} + (C_5 UA_{overall,evap,sh} + C_6) w_{evap,sh} \quad (2)$$

The coefficients of Eq. (2) can be found in the appendix and the calculation of the component model variables can be found in Cheung and Braun (2012). The charge tuning was conducted with 92 data points. Since a majority of the data were collected at standard charge, the cost function was weighted as shown in Eq. (3) according to charge levels, to avoid overemphasis on the standard charging condition where n is the number of charge levels and N_j is the number of cases at the j^{th} charge level. The optimization process is explicitly constrained such that an increase in condenser subcooled region increases the amount of charge while an increase in evaporator superheated section lowers the estimated charge. This ensures that the subcooling increases with the amount of charge, and superheat decreases as charge is increased, which is commonly found in the field.

$$J = \Sigma_{j=1}^{n} \frac{\Sigma_{i=1}^{N_j} (M_{mea,i} - \hat{M}_{mea,i})^2}{N_j} \tag{3}$$

Results for charge tuning based on Eq. (1) are plotted in Figure 2, showing a maximum deviation of 13% and a coefficient of determination 0.9319. Results for the modified charge tuning method are shown in Figure 2, with a maximum deviation of 8% and a coefficient of determination 0.9573. Despite the higher maximum deviation, the higher coefficient of determination and the smaller bias for high charge values in Figure 2 show that the new charge tuning equation improves the model.

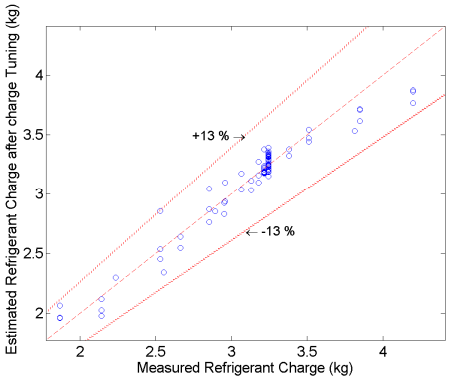

Figure 1: Charge tuning results based on Eq. (1)**.**

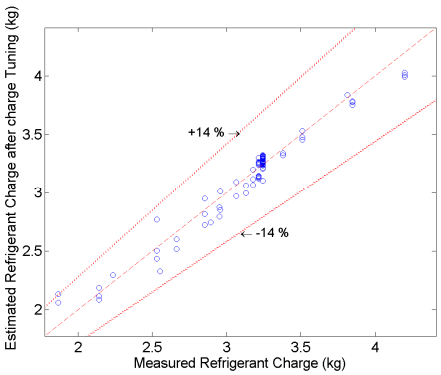

Figure 2: Charge tuning results based on Eq.(2).

4. FAULT MODELING

Modeling of non-standard charging can be done by imposing a different charge. When modeling evaporator fouling, the airflow across the evaporator was reduced as Yang *et al.* (2006) suggested that the evaporator filter fouling lowered the airflow. Bell et al. (2012) also showed that heat exchanger fouling increased the pressure drop and to simulate the condenser fouling effect for constant speed fans, the airflow across the condenser can be reduced. However, the component models needed to be modified when considering compressor valve leakage, liquid line restriction and the existence of non-condensable gas in the refrigerant circuit. In this paper, compressor valve leakage and liquid line restriction modeling are discussed.

4.1 Compressor valve leakage

Compressor valve leakage is a consequence of incomplete closure of a damaged compressor valve in each compression cycle. A leaky discharge valve leads to high pressure and temperature gas leaking back into the compression chamber from the discharge line during a portion of the compression cycle. A leaky suction valve causes gas to leak from the compression chamber to the suction line during a portion of the compression process. In either case, the compressor produces less flow and operates at a higher discharge temperature for a given suction and discharge pressure. Compressor valve leakage was simulated experimentally by Kim *et al.* (2009) by bypassing some refrigerant from the compressor discharge to suction. The same approach was used in simulation by changing the inputs to the compressor model described in Cheung and Braun (2012) as shown in Eqs. (4) and (5), which the compressor valve leakage level is defined as the ratio of the change of refrigerant mass flow due to compressor valve leakage to the original mass flow rate.

$$\dot{m}_{r,final} = (1 - VL)\dot{m}_{r,initial} \tag{4}$$

$$h_{r,comp,out} = f_{comp}(P_{r,in}, P_{r,out}, h_{r,comp,in} = h_{r,suctionline,out}(1-VL)+h_{r,comp,out}VL) \quad (5)$$

4.2 Liquid Line Restriction

Liquid line restrictions can be caused by accumulation of impurities in the filter/drier or by crimps or sediment in the refrigerant pipelines between the condenser and the expansion valve outlet. Breuker (1999) defines the fault level as the ratio of the pressure drop caused by the fault to the refrigerant pressure difference between the condenser outlet and the expansion valve outlet without the restriction. Since the fault level is an input to the model, the model needs to simulate operation without the liquid line restriction first to obtain the denominator. The simulation is repeated with the known restriction pressure drop. The resultant model is presented in Eq. (6).

$$\begin{aligned} P_{r,liquidline,out} = \quad & P_{r,liquidline,out}|_{\text{from liquid line model}} \\ & -\text{LL\_level}(P_{r,liquidline,in} - P_{r,FEO,out}) \end{aligned} \quad (6)$$

5. RESULTS AND DISCUSSION

5.1 Comparison with experimental data

The evaporator heat transfer rates and the corresponding residual plot obtained from system simulations and air-side measurements are shown in Figure 3 and Figure 4. These results include all data from the experiments, except a few cases having both condenser fouling and subcooling less than 3K.

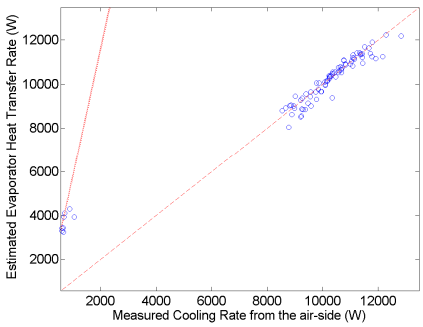

Figure 3: Simulated evaporator heat transfer rate compared to air-side measurements.

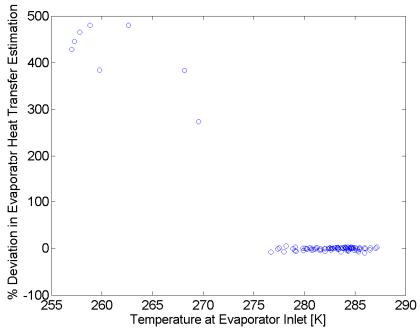

Figure 4: Residual heat transfer rate as a function of refrigerant temperature at evaporator inlet.

Figure 3 shows a large deviation between the measurement and simulation in some low-load cases. It is a consequence of below freezing conditions on the evaporator as demonstrated by larger residuals at subfreezing temperatures in Figure 4. The evaporator model in Cheung and Braun (2012) assumes that the humidity in the air will not freeze up on the coil and the effect of frost on coils is not captured accurately when the surface temperature of the coil is below freezing. The out-of-range estimation results in a large deviation between the measurement and simulation. The experimental comparison excluding these scenarios, which are undercharged refrigerant cases, is shown in Figures 5 to 8.

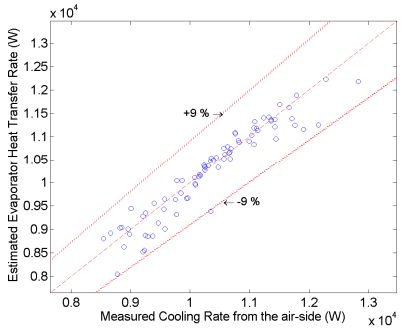

Figure 5: Simulated evaporator heat transfer rate without subfreezing evaporator coil conditions.

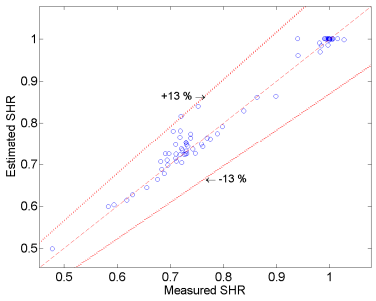

Figure 6: Simulated sensible heat ratio without subfreezing evaporator coil conditions.

From Figure 5 to Figure 8, the simulated evaporator heat transfer rates, sensible heat ratios, compressor power consumption, and condenser heat transfer rate differ from the experimental data by a maximum of 9%, 13%, 7% and 5%, respectively, with mean deviations of 6%, 4%, 3% and 5% respectively. During the parameter estimation process in Cheung and Braun (2012), the refrigerant-side evaporator heat transfer rate was used instead of the air-side. However, since some experimental data do not have enough superheat for refrigerant-side measurement, air-side heat transfer rate, which is 2.16% higher than the refrigerant-side data on average, is used for comparison. This creates a bias in Figure 5 whereas the result in Figure 6 is similar to the sensible heat ratio distribution estimated in Cheung and Braun (2012). Overestimations in compressor power and condenser heat transfer rates are observed in Figure 6 and Figure 7 which is caused by an overestimation in high-side pressure and the assumption that refrigerant is not stored within the oil of the compressor. In Cheung and Braun (2012), the liquid line measurements showed negative pressure drops in a majority of cases. Since the model cannot account for the negative pressure drops, it predicts higher compressor discharge pressures. This increases the compressor power consumption and the condenser heat transfer rate. The bias is intensified because the model neglects the amount of charge absorbed in the compressor sump oil. From Shen (2006) simulation results, the amount of refrigerant in the compressor oil ranges from 8% at ordinary charge levels to 12% at overcharged levels. Since the charge tuning equation neglects the compressor effect at different charge levels, more of the charge participates in the simulated overcharged cases than occurred for the actual system leading to even higher predicted high-side pressures relative to the measured values.

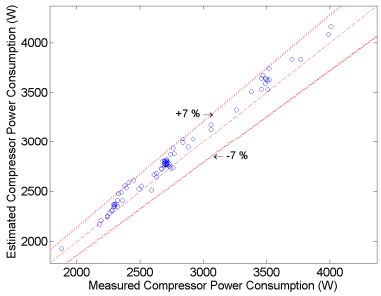

Figure 7: Simulated compressor power consumption without subfreezing evaporator coil conditions.

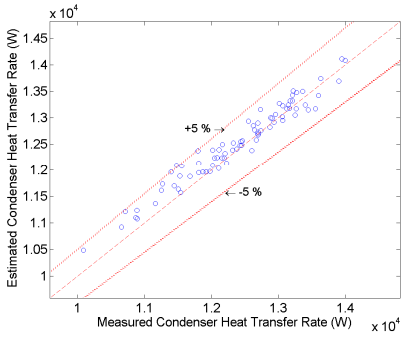

Figure 8: Simulated condenser heat transfer rate without subfreezing evaporator coil conditions.

5.2 Simulation under non-standard charge conditions

A comparison between model predictions and experimental values was made at various charging levels, with indoor dry-bulb temperature at 26.7°C, indoor relative humidity at 51% and ambient temperature at 35°C. The results are shown in Figure 9 to Figure 12.

Figure 9 to Figure 12 show that the trends of the variables are captured correctly as charge varies. When charge level increases, subcooling and refrigerant pressures increase because of the increase in the average density of refrigerant inside the system. This drives down the amount of refrigerant vapor in the system and decreases the superheat at the compressor suction.

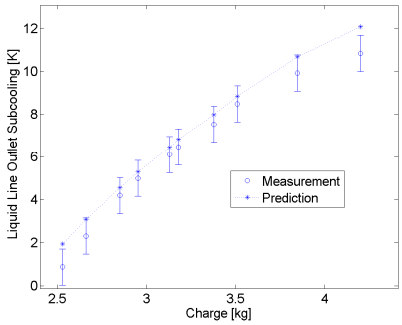

Figure 9: Subcooling with various refrigerant charge levels.

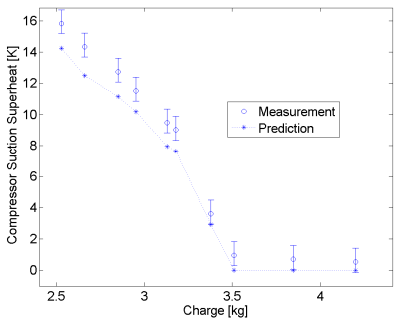

Figure 10: Superheat with various refrigerant charge levels.

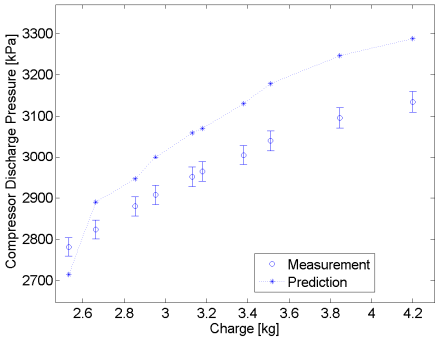

Figure 11: Compressor discharge pressure with various refrigerant charge levels.

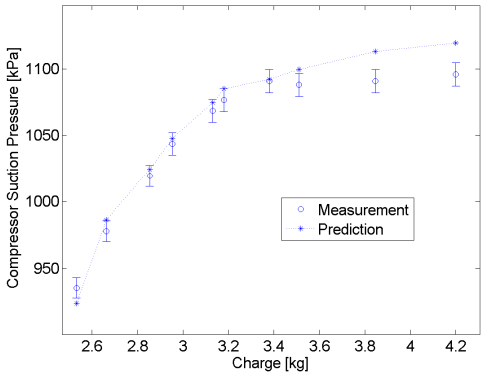

Figure 12: Compressor suction pressure with various charge levels.

5.3 Simulation under evaporator fouling

The effect of simulated evaporator fouling on system performance under the same conditions as in Section 5.2 is shown in Figure 13 to Figure 16.

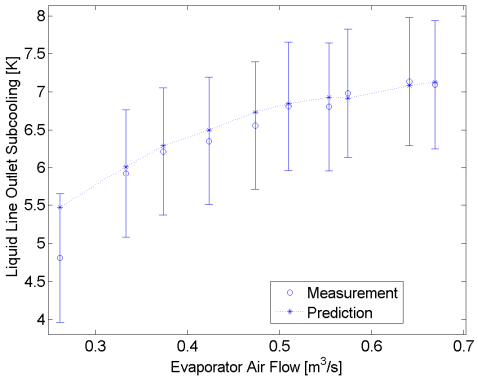

Figure 13: Subcooling with evaporator fouling.

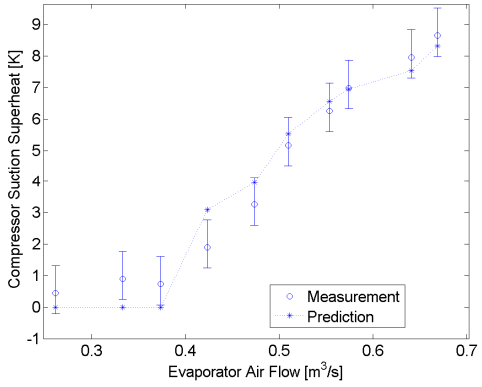

Figure 14: Superheat with evaporator fouling.

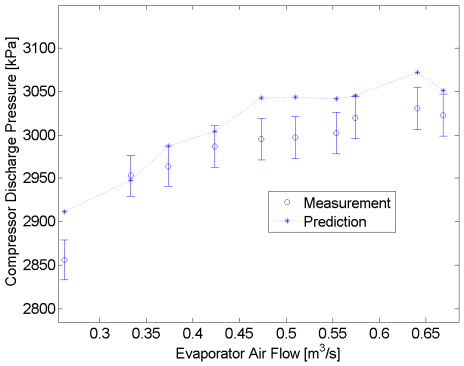

Figure 15: Compressor discharge pressure with evaporator fouling.

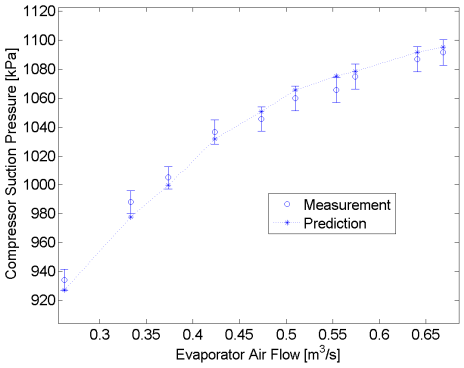

Figure 16: Compressor suction pressure with evaporator fouling.

Figure 13 to Figure 16 show that the trends of the simulation results generally follow the experimental data. When the evaporator air flow decreases, the heat transfer to the evaporator is reduced. This decreases the temperature and

pressure of the refrigerant on the low-pressure side of the system. It also lowers the density at the compressor suction, the refrigerant mass flow rate and the evaporator superheat. The lower refrigerant flow and evaporator heat transfer lead to lower compressor power consumption and the heat rejection from the condenser. The smaller condenser heat transfer reduces the temperature difference between the ambient and the condenser and the corresponding refrigerant pressure. The decrease of condensing pressure leads to lower condenser subcooling.

5.4 Simulation with condenser fouling

The effect of simulated condenser fouling is shown from Figure 17 to Figure 20, as measured with indoor dry-bulb temperature at 26.7°C, indoor relative humidity at 51%, and ambient temperature at 27.8°C. The trends of the measurements and predictions follow each other as the condenser fouling level increases. Condenser fouling increases the temperature difference between the condenser refrigerant and ambient and raises the high-side pressure. This causes a decrease in subcooling and superheat, and an increase in low-side pressure as condenser fouling intensifies.

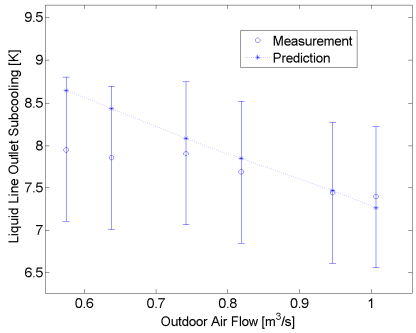

Figure 17: Subcooling with Condenser Fouling.

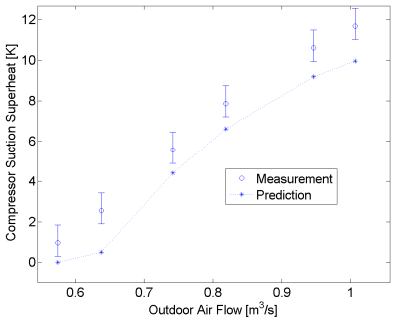

Figure 18: Superheat with Condenser Fouling.

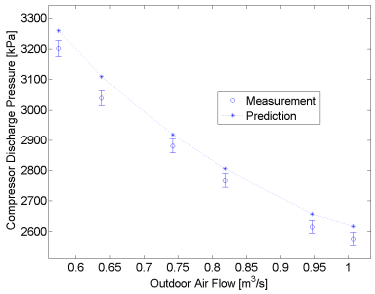

Figure 19: Compressor Discharge Pressure with Condenser Fouling.

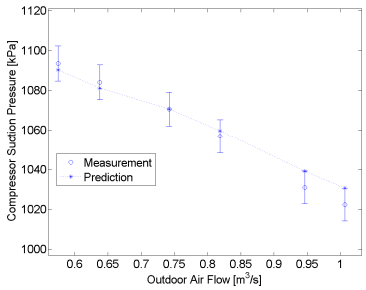

Figure 20: Compressor Suction Pressure with Condenser Fouling.

5.5 Simulation with compressor valve leakage and liquid line restriction model

Since the measurements from Shen (2006) did not include compressor valve leakage or liquid line restriction faults, the models were used to predict the effect of these faults on the system without direct experimental validation. Figure 21 and Figure 22 show the Pressure-enthalpy (P-h) diagrams of the faults effects at an indoor dry-bulb temperature of 26°C, dewpoint of 5.9°C and ambient dry-bulb temperature of 46°C, with standard charge level and airflows.

The compressor valve leakage fault results in Figure 21 indicate that cycle depicted on a T-s diagram shrinks towards the center. The refrigerant mass flow rate also decreases, as suggested by Eq. (4). This causes a drop in cooling rate and compressor power consumption as the fault level increases. Figure 22 shows that the liquid line restriction causes an increasing pressure drop across the system with an expansion of the P-h diagram towards the bottom. This increases the superheat significantly as the fault level increases and hence a reduction in the coefficient of performance.

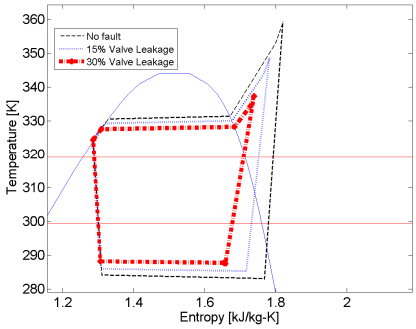

Figure 21: T-s diagram for compressor valve leakage scenarios.

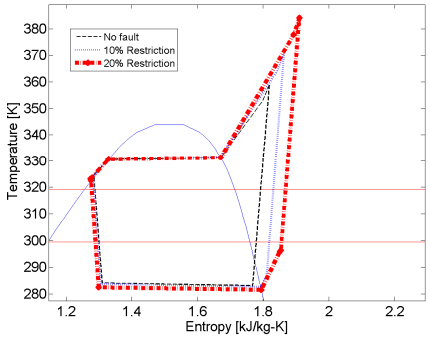

Figure 22: T-s diagram for liquid line restriction scenarios.

Breuker (1997) reported important measurements for a fixed orifice system under liquid line restriction and compressor valve leakage and the trends compare favorably with those predicted in Figure 21 and Figure 22. Experiments showed increasing compressor valve leakage increased the evaporating temperature and decreased the superheat, which is also the case in Figure 21. Significant increases in superheat and compressor discharge temperature were also observed in the experiments for liquid line restrictions, which agree with trends in Figure 22.

5.6 Solver guess values and calculation speed

To assess the speed of the solver fairly, appropriate initial guess values, rather than the experimental results, should be used. To generate appropriate initial guesses, empirical formulas relating inputs to the system and the independent variables to the solver in Table 1 were constructed and are presented Eq. **(7)** where the coefficients are given in the appendix, which provides seven coefficients for each of the six independent variables.

$$\begin{aligned}\text{Solver inputs} = \quad & C_7 + C_8 T_{a,in,evap} + C_9 TD_{a,in,evap} + C_{10}\dot{V}_{a,in,evap} \\ & + C_{11} T_{a,in,cond} + C_{12}\dot{V}_{a,in,cond} + C_{13} M\end{aligned} \tag{7}$$

From the simulations on 393 convergent cases with random environmental conditions within the range of experimental cases, the CPU time to solve one cycle scenario, without any parallel computation within the algorithm, averaged 20.15s with a standard deviation 11.20s on a computer with 2.70 GHz quad-core processor and 6.0 GB of installed memory, excluding the input-output time. The maximum calculation time was 97.45s and the minimum time was 11.61s. This model runs much faster than forward models that are based on a finite volume approach within the heat exchangers.

6. CONCLUSIONS

In this paper, the component models presented in Cheung and Braun (2012) were combined together for rapid simulation of a complete vapor compression cycle. An earlier charge tuning method was improved and utilized to tune the model to estimate the effects of charge more accurately. Models capable of simulating the effect of heat exchanger fouling, incorrect refrigerant charge, compressor valve leakage and liquid line restrictions were developed. Detailed validation results were presented for the heat exchanger and charge faults, whereas the trends with respect to compressor valve leakage and liquid line restriction faults agree with previous results published in the literature. Additional validation will be performed for other units in the future. Modifications are still needed to improve convergence at low charge cases and to include the effect of charge absorbed within the compressor oil.

NOMENCLATURE

C	coefficients	(varies)	**Subscripts**	
h	enthalpy	(J/kg-K)	a	air
J	cost function	(--)	comp	compressor
LL_level	liquid line restriction level defined in section 4.2	(--)	cond	condenser
M	amount of charge	(kg)	evap	evaporator

m	mass flow rate	(kg/s)	FEO	fixed orifice
N_j	number of data points at the j^{th} charge level	(--)	final	after tuning/adjusted
n	number of charge levels	(--)	in	inlet
P	pressure	(kPa)	initial	before tuning/adjusted
SC	condenser subcooling	(K)	liquidline	liquid line
SH	compressor superheat	(K)	mea	measured
T	temperature	(K)	out	outlet
UA	heat transfer conductance	(W/K)	overall	overall
V	airflow	(m^3/s)	r	refrigerant
VL	compressor valve leakage level defined in section 4.1	(--)	sc	subcooled
w	area ratio	(--)	sim	simulated
			sh	superheated
			suctionline	suction line

REFERENCE

Bell, I.H., Groll, E.A., König, H., 2012, Experimental Analysis of the Effects of Particulate Fouling on Heat Exchanger Heat Transfer and Air-Side Pressure Drop for a Hybrid Dry Cooler, *Heat Transf. Eng.*, vol. 32 no. 3–4: p. 264–271.

Breuker, M., 1997, *Evaluation of a Statistical, Rule-based, Detection and Diagnostics Method for Vapor Compression Air Conditioners*, Master thesis, Ray W. Herrick Laboratories, Purdue University, Ind. Report No. 1796-6

Cheung, H. and Braun, J. E., 2012, "Inverse Modeling to Simulate Fault Impacts for Vapor Compression Equipment Part 1: Component Modeling and Validation", *Proceedings of the 15th International Refrigeration and Air Conditioning Conference at Purdue*, West Lafayette, IN

Harms, T. M., 2002, *Charge Inventory System Modeling and Validation for Unitary Air Conditioners*, PhD. thesis, Ray W. Herrick Laboratories, Purdue University, Ind. Report No. 5288-2

Kim, M., Payne, W. V., Domanski, P. A., Yoon, S. H., Hermes, C. J. L., 2009, "Performance of a Residential Heat Pump Operating in Cooling Mode with Single Fault Imposed", *Applied Thermal Engineering*, 29: 770 - 778

LeRoy, J. T., 1997, *Capacity and Power Demand of Unitary Air Conditioners and Heat Pumps Under Extreme Temperature and Humidity Conditions*, Masters thesis, Ray W. Herrick Laboratories, Purdue University, Ind. Report No. 3220-2

Payne, W. V, O'Neal, D. L., 1999, "Multiphase Flow of Refrigerant R410A Through Short Tube Orifices", *ASHRAE Transactions*, 105 (2): 66 – 74

Rossi, T. M., 1995, *Detection, Diagnostics, and Evaluation of Faults in Vapor Compression Equipment*, PhD thesis, Ray W. Herrick Laboratories, Purdue University

Shen, B., 2006, *Improvement and validation of unitary air conditioner and heat pump simulation models at off-design conditions*, Ph.D. thesis, Ray W. Herrick Laboratories, Purdue University, Ind. Report No. 6304-1 HL2006-1

Yang, L., Braun, J.E., Groll, E.A., 2007, The impact of fouling on the performance of filter-evaporator combinations, Int. J. Refrigeration, vol. 30 (2007), p. 489-498.

Yuill, D.P, Braun, J.E., 2012, "Evaluating Fault Detection and Diagnostics Protocols Applied to Air-cooled Vapor Compression Air-conditioners", *Proceedings of the 15th International Refrigeration and Air Conditioning Conference at Purdue*, West Lafayette, IN

ACKNOWLEDGEMENT

The authors acknowledge National Institute of Standards and Technology (NIST) Grant # 104867 for sponsoring the project development. The authors are also thankful for the help of David Yuill from Purdue University and Drs. Vance Payne and Piotr Domanski from NIST on this project.

APPENDIX

Table A.1: Coefficients in Eq. (2).

Charge Tuning Equation	C_0 [kg]	C_1 [kg-K/W]	C_2 [kg]	C_3 [kg-K/W]	C_4 [kg]	C_5 [kg-K/W]	C_6 [kg]
	1.1352	0.0046	-1.7645	-0.0033	1.2216	0.001	-0.3774

Table A.2: Coefficients in Eq. (7).

Independent variables	$P_{r,sat,comp,out}$		$P_{r,sat,comp,in}$		$SH_{evap,out}$
C_7 [kPa]	-4.66E+03	C_7 [kPa]	-1.45E+04	C_7 [K]	-4.60E+01
C_8 [kPa/K]	5.75E+00	C_8 [kPa/K]	-1.49E+01	C_8 [--]	3.94E-01
C_9 [kPa/K]	4.55E+00	C_9 [kPa/K]	2.83E+00	C_9 [--]	3.37E-01
C_{10} [kPa-s/m^3]	9.30E+01	C_{10} [kPa-s/m^3]	2.47E+01	C_{10} [K-s/m^3]	1.73E+01
C_{11} [kPa/K]	7.89E+00	C_{11} [kPa/K]	7.03E+01	C_{11} [--]	-4.89E-01
C_{12} [kPa-s/m^3]	-3.09E+02	C_{12} [kPa-s/m^3]	-1.07E+03	C_{12} [K-s/m^3]	1.62E+01
C_{13} [kPa/kg]	1.72E+02	C_{13} [kPa/kg]	1.67E+02	C_{13} [K/kg]	-1.24E+01
Independent variables	($P_{r,comp,out}$ - $P_{r,FEO,in}$)		($P_{r,FEO,out}$ - $P_{r,suctionline,out}$)		$SC_{FEO,in}$
C_7 [kPa]	-1.00E+02	C_7 [kPa]	-1.33E+02	C_7 [K]	-6.31E+01
C_8 [kPa/K]	1.63E+00	C_8 [kPa/K]	2.97E-01	C_8 [--]	1.99E-01
C_9 [kPa/K]	6.93E-01	C_9 [kPa/K]	-4.36E-02	C_9 [--]	8.63E-02
C_{10} [kPa-s/m^3]	4.77E+01	C_{10} [kPa-s/m^3]	1.41E+00	C_{10} [K-s/m^3]	3.35E+00
C_{11} [kPa/K]	-1.89E+00	C_{11} [kPa/K]	2.27E-01	C_{11} [--]	-1.10E-01
C_{12} [kPa-s/m^3]	1.96E+00	C_{12} [kPa-s/m^3]	-1.20E+01	C_{12} [K-s/m^3]	-6.45E-01
C_{13} [kPa/kg]	1.68E+01	C_{13} [kPa/kg]	1.03E+01	C_{13} [K/kg]	5.37E+00

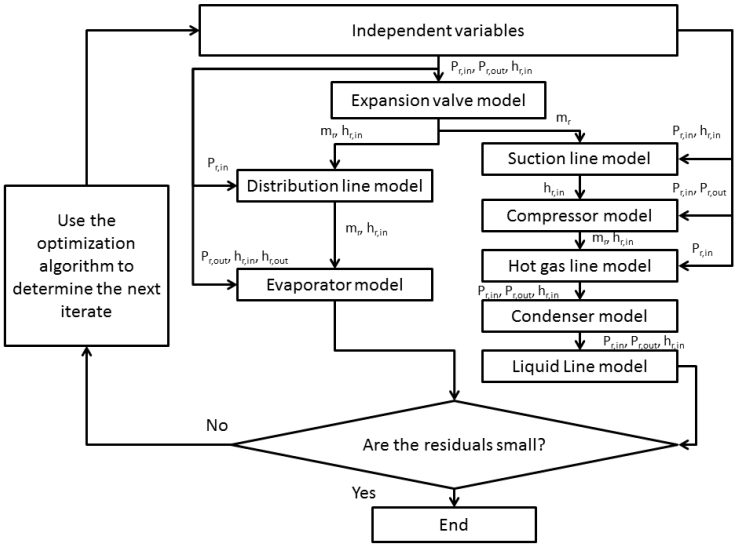

Figure A.1: Solution process of the cycle solver.